Density-of-States-Based Physical Model for Ink-Jet Printed Thiophene Polymeric TFTs

Jiyoul Lee, Jun Tae Jang, Jaeman Jang, Jaehyeong Kim, Jong Won Chung, Sung-Jin Choi, Dong Myong Kim, Kyung Rok Kim, *Member, IEEE*, and Dae Hwan Kim, *Senior Member, IEEE*

***Abstract*— We proposed a physical model for ink-jet printed polymeric thin-film transistors (PTFTs) all over the sub- and above-threshold regions by using an effective carrier density. The nonlinearity under the low lateral electric field in the printed thiophene PTFTs was reproduced by applying the back-to-back Schottky diode model based on simple Poole–Frenkel (PF) mobility formalism. The analytical *I–V* model supplemented with *C–V* model in a single framework was also verified by successfully reproducing the measured characteristics of TFTs with three different thiophene polymeric channel materials. Additionally, we applied the physics-based analytical model on the inkjet-printed PTFT-based inverter and confirmed that the proposed models could predict the inverter circuit characteristics of the gain and static noise margin (SNM) based on the physical parameters.**

***Index Terms*— Analytical model, effective carrier density, inverter, nonlinearity, polymer, Poole–Frenkel (PF), Schottky, thin-film transistors (TFT).**

I. Introduction

ORGANIC thin-film transistors (OTFTs), where organic semiconductors, including small-molecule (oligomer) and macromolecule (polymer), are served as active channel materials, are under intensive research and development for applications in large-area and flexible electronics due to their low-temperature and low-cost printing fabrication capability [1]. In spite of the advantage of the simple solution-based process, however, the organic semiconductors have been hard to be characterized with a widely accepted model owing to the lack of physical understanding and their process-dependent variations showing the wide-range of mobility (10^{-5} ~ 10 cm^2/Vs) [2], [3]. Especially, considering the impact of their industrial applications, the models should be supplemented for high mobility (~1 cm^2/Vs) organic channel materials.

Since the pioneering work of the analytical model for the charge transport in the organic semiconductors has been performed by using single trap level near band-edge [4], there have been much elaborate efforts on the trap-related analytical models for short channel OTFTs with an equivalent circuit [5], mobility extractions based on the various distribution of subgap density-of-states (DOSs) from organic semiconductors [6]–[9] in terms of the process- and material-dependent organic channel characterization. However, although all of these analytical approaches retain their physical validity at the moment, many controversial arguments that are deviated from the given physical model have arisen since high mobility organic semiconductors where non-linear or super-linear transport is dominant under specific condition have been recently reported [10], [11]. Therefore, it is still necessary to develop the physics-based and widely-applicable analytical model with more details for carrier transport in various organic channel materials, which can be advanced for predictable OTFT circuit design toward the compact models [12]–[14].

In addition to the channel modeling in OTFTs, the contact resistance modeling is another important issue to describe the non-linearity under small drain bias, which has been originated from the inherent Schottky contact formation in OTFTs due to the limited doping process for ohmic contact [15], [16]. While Schottky contact resistance in OTFTs has been modeled by the antiparallel Schottky diode model assuming its barrier height [17], [18] or investigated by the physical barrier height [19], the complete Schottky contact modeling with experimentally extracted or physical barrier height incorporated into the analytical model has been rarely developed. As an initial work, we presented a numerical and analytical model [20], [21], and extended to circuit-level simulation for a specific polymer channel material [22].

In this work, we developed an analytical OTFT model that is verified by three different thiophene-based polymeric TFTs (PTFTs) with P3HT, short for regioregular poly(3-hexylthiophene), PQT-12, short for poly(3,3‴-didodecylquaterthiophene), as well as P(8T2Z-co-6T2Z)-12, short for poly[(tetryldodecyloctathiophene-*alt*-didodecylbithiazole)-

Manuscript received September 11, 2019; revised October 29, 2019; accepted November 8, 2019. Date of publication December 10, 2019; date of current version December 30, 2019. This work was supported by the National Research Foundation of Korea (NRF) through the Korean Government [Ministry of Education, Science and Technology (MEST)] under Grant 2016R1A5A1012966, Grant 2017R1A2B4006982, Grant 18ZB1800, Grant 2016M3A7B4909668, and Grant 2018R1A1A1A05021060. The review of this article was arranged by Editor Y. Noh. *(Jiyoul Lee and Jun Tae Jang contributed equally to this work.) (Corresponding authors: Kyung Rok Kim; Dae Hwan Kim.)*

J. Lee is with the Department of Graphic Arts Information Engineering, Pukyong National University, Busan 48513, South Korea.

J. T. Jang, J. Jang, J. Kim, S.-J. Choi, D. M. Kim, and D. H. Kim are with the School of Electrical Engineering, Kookmin University, Seoul 02707, South Korea (e-mail: drlife@kookmin.ac.kr).

J. W. Chung is with the Material Research Center, Samsung Advanced Institute of Technology, Suwon 16678, South Korea.

K. R. Kim is with the School of Electrical and Computer Engineering, Ulsan National Institute of Science and Technology, Ulsan 44919, South Korea (e-mail: krkim@unist.ac.kr).

Color versions of one or more of the figures in this article are available online at http://ieeexplore.ieee.org.

Digital Object Identifier 10.1109/TED.2019.2953193

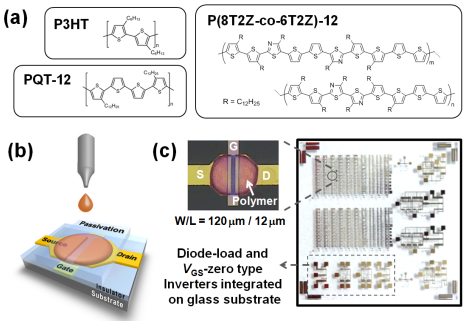

Fig. 1. (a) Three different types of polymer semiconductor inks used in this study; P3HT, PQT-12, and P(8T2Z-co-6T2Z)-12. (b) Schema of the coplanar structured PTFT fabricated with inkjet-printing. (c) Optical images of the fabricated PTFTs and the integrated diode-load and V_{GS}-zero type inverters on a glass substrate.

co-(tetryldodecylhexathiophene-*alt*-didodecylbithiazole)] as an active channel layer [Fig. 1(a)] [20]–[23]. In detail, analytical $I-V$ model incorporating DOS-controlled effective mobility model considering physical trap-related effective carrier density based on the observation of a field-dependent Poole–Frenkel (PF) effect (Section III-A), back-to-back Schottky diode model with physical barrier height for the nonlinearity under small drain bias (Section III-B), and analytical $C-V$ model describing the junction depletion and gate capacitance (Section IV) are developed in a single framework of the analytical model. Moreover, the DOS-based circuit characteristics of PTFT inverters are successfully investigated and predicted from circuit simulation by using the proposed model (Section V).

II. Device Fabrication Process

For the experimental verification, we fabricated the coplanar structured PTFTs by using ink-jet printing [Fig. 1(b)] and integrated inverters on a glass substrate [Fig. 1(c)]. The sputter-deposited molybdenum (Mo) was photolithographically patterned for a gate electrode. Then, a 300-nm-thick silicon dioxide (SiO_2, $C_{ox} = 10$ nF/cm^2) was deposited by plasma-enhanced chemical vapor deposition (PECVD) as the gate dielectric. The source and drain electrodes (Au: thickness ~50 nm) were deposited by e-beam evaporation and patterned again by photolithography. Before inkjet-printing of the polymer semiconductor inks, the surface of the gate dielectric was treated with octadecyltrichlorosilane (ODTS) self-assembled monolayer (SAM) for a hydrophobic channel area. Three types of polymer semiconductor inks [0.2 wt% in Tetralin (1,2,3,4-tetrahydronaphthalene)] were printed by Dimatix inkjet-printer to form an active layer [20]–[23] and annealed at 150 °C for 1 h in N_2 ambient. The thickness of all the polymer films ($T_{polymer}$) was confirmed to be ~30 nm by the focused ion-beam scanning electron microscope (FIB-SEM). The bandgap (E_g) that is being synthesized in the polymer semiconductor has dependence upon the type and fabricating condition of the molecule, as well as the material property of the gate insulator. Here, it was used E_g of 1.9 eV, permittivity of $3 \times \varepsilon_0$, 8.5×10^{18} cm^{-3} eV^{-1} for the effective hole density of state (N_V) [24], and the measured values of $C-V$ for doping concentration (N_A) [25]. Typical

TABLE I
Structural and Extracted Model Parameters for Analytical $I-V$ Model With Different Channel Materials

Parameter	P3HT	PQT-12	P(8T2Z-co-6T2Z)-12
W/L [μm]	120/12	120/12	120/12
$T_{OX}/T_{Polymer}$ [nm]	300/50	300/50	300/50
μ_{Band} [cm^2/V·s]	0.015	0.025	0.146
N_A [cm^{-3}]	1.7×10^{17}	2.5×10^{17}	3.0×10^{18}
C_{OX} [nF/cm^2]	17.36	17.36	17.36
m^*_P [kg]	$m_0/4$	$m_0/4$	$m_0/4$
$q\cdot\phi_B$ [eV]	0.35	0.31	0.25
V_{FB} [V]	2	2	-1.5
ε [F/cm]	$3\varepsilon_0$	$3\varepsilon_0$	$3\varepsilon_0$

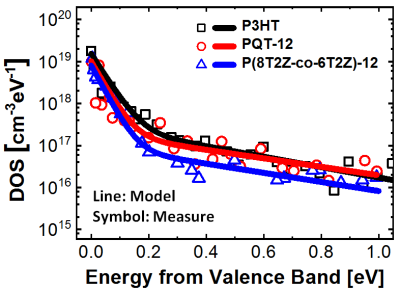

Fig. 2. Plots of DOS versus energy from valence band for the respective polymer semiconductor; P3HT, PQT-12, and P(8T2Z-co-6T2Z)-12.

geometric parameters of used devices are listed in Table I. Electrical measurements of the PTFTs were performed with Agilent 4284A *LCR* meter and 4156C semiconductor analyzer for $C-V$ and $I-V$ characteristics, respectively.

III. Analytical $I-V$ Model

A. DOS-Controlled Effective Mobility Model

For the polymer channel layers, the energy-dependent donor-like DOS [g_D(E)] over the bandgap is modeled as a superposition of exponential deep and tail states as follows:

$$g_D(E) = N_{TD}e^{(E_V-E)/kT_{TD}} + N_{DD}e^{(E_V-E)/kT_{DD}} \quad (1)$$

where E_V is the valence band maximum, $N_{TD}(N_{DD})$ and $kT_{TD}(kT_{DD})$ are the effective density of states and the characteristic energy, respectively, for the donor-like tail (deep) states in the valence band. Note that a Gaussian DOS is actually better to represent disordered polymer semiconductors. However, the exponential DOS is still applicable for highly crystalline thiophene-based polymer semiconductors used in this study [20]. Fig. 2 shows the extracted DOS curves of three different polymer semiconductors from the multi-frequency $C-V$ spectroscopy and their fit curves with the model (1) [20]–[22]. Assuming that the trapped holes p_{tail} in the tail states dominate the localized hole density $p_{loc}(= p_{deep} + p_{tail})$ in g_D(E) since the bulk Fermi-level E_F at the thermal equilibrium is close to E_V, the trapped holes

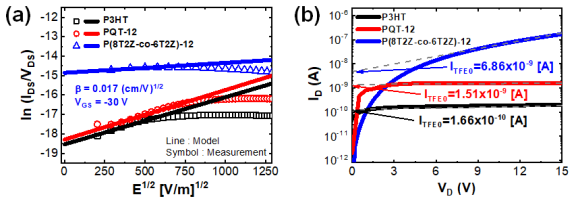

Fig. 3. (a) Plot of $ln\,(I_{DS}/V_{DS})$ versus $|V_{DS}|^{1/2}$ from the measured data in the PTFTs of P3HT, PQT-12, and P(8T2Z-co-6T2Z)-12. The straight lines fit for the curves in high V_{DS}. (b) Measured I–V characteristics of PTFT with source-polymer-drain region modeled as a back-to-back Schottky diode while the gate bias V_G is not applied (floating).

p_{loc}, as well as free holes p_{free} in the valence band, can be expressed as [24]

$$p_{loc} \cong p_{tail} = N_{TD} kT f(T, T_{TD}) \times \exp(-q(\phi(x) - V_{CH}(y) - \phi_{F0})/kT_0)$$

where

$$f(T, T_{TD}) = \begin{cases} \pi / \sin(\pi T/T_{TD}), & T_0 = T_{TD} : T < T_{TD} \\ (T/T_{TD} - 1)^{-1}, & T_0 = T : T > T_{TD} \end{cases} \quad (2)$$

$$p_{free} = N_V \exp(-q(\phi(x) - V_{CH}(y) - \phi_{F0})/kT) \quad (3)$$

where $\phi(x)$ is the potential across the polymer layer, $V_{CH}(y)$ is the lateral potential along the channel, and $q\phi_{F0}$ is E_F–E_V. To describe the gate bias (V_{GS})-dependent charge density $\rho(x)$ in the polymer, we propose the effective hole density $p_{effi}(x)$ as

$$p_{effi}(x) \equiv N_{effi} \exp\left(-q(\phi(x) - V_{CH}(y) - \phi_{F0})/kT_{effi}\right), \quad i = 1 \text{ or } 2 \quad (4)$$

$$\frac{\rho(x)}{q} \approx \begin{cases} p_{tail} \equiv p_{eff1}(x): & V_T < V_{GS} < V_{FB} \\ p_{tail} + p_{free} \equiv p_{eff1}(x): & V_{GS} \approx V_T \\ p_{free} \equiv p_{eff2}(x): & V_{GS} < V_T \end{cases} \quad (5)$$

where N_{effi} is the effective hole density in the valence band, and kT_{effi} is the effective characteristic energy with $i = 1$ or 2 for the sub- or above-V_T region. So, from the 1-D Poisson's equation of $\partial^2\phi(x)/\partial x^2 = -qp_{effi}(x)/\varepsilon_P$ based on the proposed effective hole density $p_{effi}(x)$, the electric field $E_P(x)$ in the polymer is obtained by using $\partial[(\partial f(x)/\partial x)^2]/\partial x = 2[\partial f(x)/\partial x]\cdot[\partial^2 f(x)/\partial x^2]$ as follows:

$$E_P(x) = -\frac{\partial\phi(x)}{\partial x} = \sqrt{\frac{2N_{effi}kT_{effi}}{\varepsilon_P}} \times \exp(-q(\phi(x) - V_{CH}(y) - \phi_{F0})/2kT_{effi}). \quad (6)$$

The free charge Q_{FREE} and total charge Q_{TOT} per unit area as a function of $\phi(x)$ can be obtained to be

$$Q_{FREE}(\phi(x)) = q\int_{\phi(x=T_P)}^{\phi(x)} \frac{p_{free}(\phi(x))}{E_P(\phi(x))} d\phi(x) = A^* \exp(qB^*(\phi(x) - V_{CH} - \phi_{F0})) \quad (7)$$

$$\text{where } A^* = \frac{N_V\sqrt{\varepsilon_P}}{B^*\sqrt{2N_{effi}kT_{effi}}}, \quad B^* = -\left(\frac{1}{kT} - \frac{1}{2kT_{effi}}\right)$$

$$Q_{ToT}(\phi(x)) = \varepsilon_P E_P(\phi(x)) = \sqrt{2\varepsilon_P N_{effi} kT_{effi}} \times \exp(-q(\phi(x) - V_{CH} - \phi_{F0})/2kT_{effi}). \quad (8)$$

Next, in order to obtain the V_{GS}- and V_{DS}-dependent channel mobility $\mu_P(\phi(x))$, we combined (7) and (8) and the equations are inserted to a field-dependent PF mobility model

$$\mu_P(\phi(x)) = \mu_{Band} \exp\left(\beta\sqrt{\frac{|V_{DS}|}{L}}\right) \frac{Q_{FREE}(\phi(x))}{Q_{ToT}(\phi(x))} \quad (9)$$

$$\text{where } \beta = \sqrt{\left(\frac{q}{kT}\right)^2 \frac{q}{\alpha\pi\varepsilon_P\varepsilon_0}}, \quad \alpha = 10$$

with μ_{Band} = the valence band mobility, β = PF factor, and α = effective field factor. Since the PF model is originated to describe the thermionic injection from the electrode to semiconductor bulk, it can explain the carrier transport from the contact to the semiconductor channel in a consistent way. Also, the PF model is simple with a relatively small number of physical parameters compared to other frequently used equations, such as the percolation model suggested by Vissenberg and Matter [25] or the Gaussian distribution model (GDM) proposed by Bässlera *et al.* [26]. Fig. 3(a) clearly shows that $ln(I_{DS}/V_{DS})$ decreases with $|V_{DS}|^{1/2}$ having linear relation, which represents that the PF effect is dominant conduction mechanism at high V_{DS} in our PTFTs.

B. Schottky Contact Model

The Schottky effect, which affects the resistance and capacitance existing the contact between metal and the polymer semiconductors, becomes more significant for the polymer semiconductor with larger output current. In order to describe the nonlinear $I-V$ characteristic in the linear region of PTFTs, the source and drain contacts to polymer channel are modeled as back-to-back connected Schottky diodes in an analytical current model. For rigorous modeling of these Schottky contacts, characterization of the Schottky barrier height (ϕ_B) was carried out through the measured $I-V$ characteristics, as shown in Fig. 3(b) with the following equations from the thermionic field emission current (I_{TFE}) [27]:

$$\phi_B = \frac{E_0}{q} \ln\left(\frac{AA^{**}T^2\sqrt{\pi E_{00}(q\phi_B)}}{I_{TFE0}kT}\right) \quad (10)$$

$$E_0 = E_{00}\coth(E_{00}/kT), \quad E_{00} = \hbar\sqrt{N_A/4m_P^*\varepsilon_P} \quad (11)$$

where A, A^{**}, T, k, $\hbar$, q, N_A, m_P^*, and ε_P are the contact area, the Richardson constant, temperature, the Boltzmann's constant, the Planck constant, the electric charge, acceptor density, the hole effective mass, and the permittivity in the polymer, respectively. With the structural and extracted model parameters summarized in Table I, we obtained the effective Schottky barrier height (ϕ_B) for each channel material. In detail, the parameter of I_{TFE0} is extracted from the thermionic field emission current equation by applying the strong lateral field in the gate floating condition [Fig. 3(b)]. Then, the parameter of ϕ_B is extracted from (1) based on the well-known $A*(= 120 \times (m_p^*/m_0))$ at room temperature as well as the previously reported and structural parameters of A, E_0, E_{00} [27]. These experimentally extracted ϕ_B confirm the Schottky contact formation in the fabricated PTFTs while the ideal contact assumption results in the ohmic contact from the known values of the electron affinity of polymer ($\chi_{polymer}$) = 3.2∼3.5 eV,

polymer bandgap (E_g) = 1.7~2.1 eV, and Au work function (WF_{AU}) = 5.1~5.47 eV. The positive physical barrier height leads to the nonlinearity under small drain bias, which will be demonstrated in the experimental results, by the following Schottky current equation ($I_{Schottky}$) as:

$$I_{Schottky} = AA^{**}T^2 \exp(-q\phi_B/\eta kT) \times (\exp(q(V_{Schottky})/\eta kT) - 1) \quad (12)$$

where η is the ideality factor, $V_{Schottky}$ is the voltage difference across the respective reverse- ($V_{Schottky\_R}$) and forward-biased ($V_{Schottky\_F}$) Schottky contact.

C. Drain Current Model

For the current equation, the drain current I_{DS} is described by

$$I_{DS} = W\frac{dV_{CH}}{dy}\mu_{Band}\exp\left(\beta\sqrt{\frac{|V_{DS}|}{L}}\right)\frac{A^*N_v}{2N_{effi}kT_{effi}C^*} \times \exp(qC^*(\phi_S - V_{CH}(y) - \phi_{F0})) \quad (13)$$

with $C^* = -(2/kT - 3/2kT_{effi})$. Gauss' law applied to the boundary between the polymer and gate insulator, gives a nonlinear relation between V_{GS} and the surface potential at polymer/gate insulator interface ϕ_S through (6) and (8) as

$$V_{GS} = V_{FB} + \phi_S + \frac{Q_{ToT}(\phi_s(y), V_{CH}(y))}{C_{ox}} \quad (14)$$

$$\frac{\partial V_{CH}(y)}{\partial \phi_S(y)} = 1 - \frac{2kT_{effi}}{q(V_{GS} - V_{FB} - \phi_S)} \quad (15)$$

with V_{FB} = the flat band voltage and C_{OX} = the oxide capacitance per unit area. By integrating (14) over the gate region for a channel $I-V$ model, the analytical drain current equation by the drift of holes in the polymer channel can be derived as

$$\begin{aligned} &I_{DS}(N_{effi}, kT_{effi}) \\ &= q\frac{W}{L}\mu_{Band}\exp\left(\beta\sqrt{\frac{|V_{DS}|}{L}}\right)\frac{A^*N_v}{2N_{effi}kT_{effi}C^*} \\ &\quad\times\int_{\phi_{SS}}^{\phi_{SD}}\left(\frac{C_{OX}(V_{GS}-V_{FB}-\phi_S)}{\sqrt{2\varepsilon_P N_{effi}kT_{effi}}}\right)^{-2C^*kT_{effi}} \\ &\quad\times\left(1-\frac{2kT_{effi}}{q(V_{GS}-V_{FB}-\phi_S)}\right)d\phi_S(y) \\ &= \frac{W}{L}\mu_{Band}\exp\left(\beta\sqrt{\frac{|V_{DS}|}{L}}\right)\frac{A^*N_v}{2N_{effi}kT_{effi}C^*} \\ &\quad\times\left(\frac{C_{OX}}{\sqrt{2\varepsilon_P N_{effi}kT_{effi}}}\right)^{-2C^*kT_{effi}} \\ &\quad\times\left[\begin{array}{l} \frac{1}{(-2C^*kT_{effi}+1)} \\ \times\{(V_{GS}-V_{FB}-\phi_{SS})^{-2C^*kT_{effi}+1} \\ \quad -(V_{GS}-V_{FB}-\phi_{SD})^{-2C^*kT_{effi}+1}\} \\ -\frac{1}{-qC^*}\left\{(V_{GS}-V_{FB}-\phi_{SS})^{-2C^*kT_{effi}}\right. \\ \qquad\left.-(V_{GS}-V_{FB}-\phi_{SD})^{-2C^*kT_{effi}}\right\} \end{array}\right]. \end{aligned} \quad (16)$$

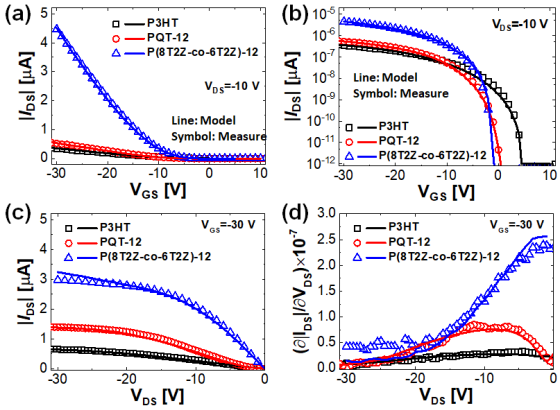

Fig. 4. $I_{DS}-V_{GS}$ characteristics in (a) linear scale and (b) semi-log scale. (c) $I_{DS}-V_{DS}$ characteristics and (d) output conductance are compared with the measured ones for the fabricated PTFT with P3HT, PQT-12, and P(8T2Z-co-6T2Z)-12.

Finally, from (16) where i = 1 or 2 denotes the respective operation regime for the sub- or above-V_T region, the channel current ($I_{DS,ch}$) for the PTFT can be expressed by the inverse limiting equation of the sub- (I_{DS_sub}) and above-V_T current (I_{DS_above}) as follows:

$$\frac{1}{I_{DS,ch}} = \frac{1}{I_{DS\_sub}(N_{eff1}, kT_{eff1})} + \frac{1}{I_{DS\_above}(N_{eff2}, kT_{eff2})} \quad (17)$$

where I_{DS_sub} and I_{DS_above} have an identical form. Since this inverse limiting equation has been originated from DOS-controlled mobility edge model, it is validated to be used in the relatively high mobility PTFTs with non-linear or super-linear transport where PF effect is dominant while it cannot be used for the transport where hopping, percolation, or multiple trapping and release (MTR), are dominant as in the conventional PTFTs with low mobility.

At this point, it should be noted that V_{DS} in (16) is different from the applied voltage from drain to source contact. In our PTFT model with back-to-back Schottky diodes and the V_{GS}-dependent channel resistance in the series connection, as shown in Fig. 1(a), the applied V_{DS} is divided into different internal voltages as $V_{DS} = V_{Schottky\_R} + V_{DS\_ch} + V_{Schottky\_F}$ for the same $I_{DS} = I_{Schottky}(V_{Schottky\_R}) = I_{DS,ch}(V_{DS\_ch}) = I_{Schottky}(V_{Schottky\_F})$. By solving these simultaneous equations, the terminal drain current as a function of the applied V_{DS} and V_{GS} having different internal voltages can be obtained as

$$\frac{1}{I_{DS}(V_{DS})} = \frac{1}{I_{DS,ch}(V_{DS\_ch})} = \frac{1}{I_{Schottky}(V_{Schottky\_R})} = \frac{1}{I_{Schottky}(V_{Schottky\_F})} \quad (18)$$

where $I_{DS,ch}$ and $I_{Schottky}$ are (17) and (3), respectively.

D. Model Versatility Verification With Experiments

The calculated transfer/output $I-V$ characteristics by the analytical model, with characteristic model parameters summarized in Table II, are well consistent with measured data from three different channel materials through Fig. 4. The

TABLE II
SUBBANDGAP DOS PARAMETERS FOR ANALYTICAL $I-V$ MODEL WITH DIFFERENT CHANNEL MATERIALS

Parameter	P3HT	PQT-12	P(8T2Z-co-6T 2Z)-12
N_V [cm^{-3}]	8.50×10^{18}	8.50×10^{18}	8.50×10^{18}
N_{eff1} [cm^{-3}eV^{-1}]	6.20×10^{18}	5.53×10^{18}	5.26×10^{18}
kT_{eff1} [eV]	0.042	0.043	0.031
N_{eff2} [cm^{-3}eV^{-1}]	1.50×10^{19}	1.00×10^{19}	1.00×10^{19}
kT_{eff2} [eV]	0.04	0.036	0.0295

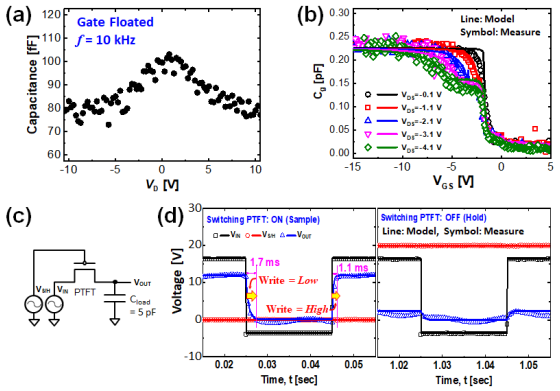

Fig. 5. (a) C–V characteristics of source-polymer-drain back-to-back Schottky diode. (b) Quasi-static C–V curves reproduced by the proposed analytical C–V model. (c) Circuit schema of the sample and hold function in 1T-1C configuration. (d) Transient characteristics of switching PTFT.

well-reproduced nonmonotonic behavior of output conductance (g_d) at low drain bias in Fig. 4(d) clearly demonstrate the nonlinearity of I_{DS}–V_{DS} characteristics under small bias through our analytical model. Thus, it is confirmed that our proposed model based on simple PF mobility formalism can be generally accepted for the description of the nonlinearity under the low lateral electric field in the highly crystalline polymer-based TFTs.

IV. ANALYTICAL C–V MODEL

In addition to the $I-V$ model, the device capacitance model considering the junction depletion and gate capacitance should be supplemented for complete transient circuit simulation as well as unit transistor simulation. In this section, $C-V$ modeling has been confirmed with measured data (Fig. 5) for PTFT with P(8T2Z-co-6T2Z)-12 as channel material, which shows the best performance with highest mobility among three different channel materials, and will be applied to the circuit simulation of PTFT based inverter in Section V.

The measured $C-V$ characteristics in Fig. 5(a) confirm the back-to-back Schottky diode modeling for the contacts by showing a symmetric depletion capacitance $C_{dep} \sim 1/(V_{bi}+V_R)^{0.5}$ over the whole reverse bias ($V_R = V_D$) range where V_{bi} is the built-in voltage in the Schottky contact [27]. For an analytical $C-V$ model in a single framework, the gate capacitance (C_G) has been derived by dQ_G/dV_{GS} based on the equation of the total gate charge Q_G. First, the total gate

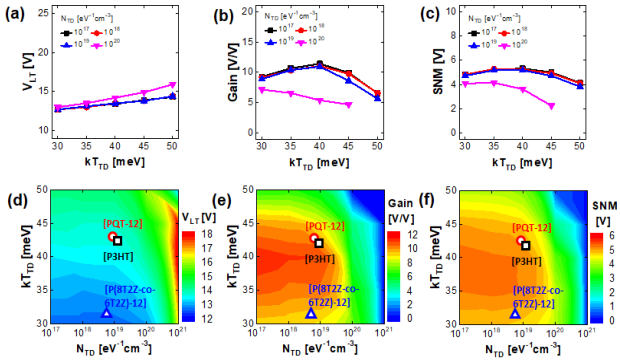

Fig. 6. Plots of (a) V_{LT}, (b) gain, and (c) SNM as a function of kT_{TD} with $N_{TD} = 1\times10^{17} \sim 1\times10^{20}$ eV^{-1} cm^{-3}. Contour plots of (d) V_{LT}, (e) gain, and (f) SNM as functions of kT_{TD} and N_{TD}.

charge Q_G has been obtained by integrating $Q_{TOT}(y)$ over the gate region from (14) as

$$Q_G = W\int_0^L Q_{ToT}(y)dy = W\int_0^L C_{OX}(V_{GS}-V_{FB}-\phi(y))dy. \quad (19)$$

Since $Q_{TOT}(y)$ is known as a function of $\phi_S(y)$, we replace the integration variable dy to $d\phi_S$, and thus, Q_G is expressed as [28]

$$Q_G = C_{OX}WL\frac{(-2kT_{eff}/q)\times A(2,1)+A(2,2)}{(-2kT_{eff}/q)\times A(2,0)+A(2,1)}$$

$$\text{where } A(n,m) = \frac{(V_{GS}-V_{FB}-\phi_{SS})^{n(-C^*)kT_{eff}+m}}{(n(-C^*)kT_{eff}+m)} - \frac{(V_{GS}-V_{FB}-\phi_{SD})^{n(-C^*)kT_{eff}+m}}{(n(-C^*)kT_{eff}+m)}. \quad (20)$$

Finally, C_G can be calculated by

$$C_G = \left.\frac{\partial Q_G}{\partial V_{GS}}\right|_{V_S,V_D=\text{const}}. \quad (21)$$

As shown in Fig. 5(b), the measured quasi-static C_G–V_{GS} curves with hump characteristics according to the increase of V_{DS} were well reproduced by the calculation results of our analytical $C-V$ model considering the depletion capacitance of back-to-back Schottky diodes in contacts [22]. In 1T-1C circuit configuration [Fig. 5(c)], the measured transient characteristics of sample/hold (S/H) function are successfully reproduced by the proposed model with well-matched writing delays [Fig. 5(d)], indicating that our solid framework of analytical $I-V$ and $C-V$ model based on the common physical parameters has been properly applied.

V. DOS-BASED PTFT INVERTER CIRCUIT SIMULATION

The analytical $I-V$ and $C-V$ models in a single unified framework are applied to the circuit simulator via Verilog-A. Here, the V_{GS}-zero type inverter is employed owing to its better gain and static noise margin (SNM) than those of diode-load type one in static random access memory (SRAM)-cell operation [22]. These device-level behaviors, according to the subgap-DOS, are expected to affect the circuit characteristics

such as the inverter gain and SNM. Fig. 6 shows the simulated inverter characteristics, including the low-transition voltage (V_{LT}) as well as the gain and SNM in voltage transfer curves of an inverter. First, V_{LT} increases as subgap-DOS increases [Fig. 6(a)] since the $|V_T|$ of PTFTs increases. Moreover, it is confirmed that V_{OUT} becomes close to V_{SS} in $V_{IN} < V_{LT}$ condition when N_{TD} increases, as expected from the V_{GS}-zero type inverter configuration where driver PTFT keeps its $V_{DS,d}$ ($= V_{OUT} - V_{SS}$) constant while both $V_{DS,l} = V_{GS,l}$ ($= V_{OUT}$) vary in load PTFT. This result provides an interesting expectation; although the increase in the $|V_T|$ of the PTFTs by the increase in the subgap-DOS concentration leads to a decrease in the current and the transconductance (g_m), the gain and SNM of inverter could be enhanced [Fig. 6(b) and (c)]. It is, mainly, because the decrease rate of the current in driver PTFT according to the increase in the subgap-DOS concentration is smaller than that of the load PTFT, and the driver and load PTFT become completely turned on and off, respectively, under $V_{IN} < V_{LT}$ condition. Therefore, the PTFTs with P3HT and PQT-12 having higher subgap-DOS can present higher inverter gain and SNM than those from PTFTs with P(8T2Z-co-6T2Z)-12 having lower subgap-DOS, as shown in Fig. 6(d)–(f). On the other hand, when the subgap-DOS continues to increase, the current (resistance) difference between the driver and the load PTFT has already become large, so that $V_{OUT} \sim V_{SS}$ in $V_{IN} < V_{LT}$ condition. In this case, as the subgap-DOS increases, the decrease in the current and g_m can cause the inverter gain and SNM to be lowered.

VI. Conclusion

The physical model for PTFTs has been proposed and verified by reproducing the measured characteristics of TFTs with three different thiophene polymeric channel materials. The effective carrier density and back-to-back Schottky diode model based on simple PF mobility formalism well reproduced the measured $I-V$ characteristics with the nonlinearity under low lateral electric field in three different ink-jet printed thiophene PTFTs for all the sub- and above-threshold regions. In addition, the unified analytical $C-V$ model with $I-V$ model in a single framework well reproduced the measured static and dynamic behaviors of the integrated PTFT circuits. We believe that our approach could provide the essential compact model platform for material/process-based optimal PTFT circuit design.

References

[1] H. Sirringhaus, "Organic field-effect transistors: The path beyond amorphous silicon," *Adv. Mater.*, vol. 26, no. 9, pp. 1319–1335, Mar. 2014.

[2] S. Himmelberger and A. Salleo, "Engineering semiconducting polymers for efficient charge transport," *MRS Commun.*, vol. 5, no. 3, pp. 383–395, Sep. 2015.

[3] X. Guo *et al.*, "Current status and opportunities of organic thin-film transistor technologies," *IEEE Trans. Electron Devices*, vol. 64, no. 5, pp. 1906–1921, May 2017.

[4] G. Horowitz and P. Delannoy, "An analytical model for organic-based thin-film transistors," *J. Appl. Phys.*, vol. 70, no. 1, pp. 469–475, Jul. 1991.

[5] L. Torsi, A. Dodabalapur, and H. E. Katz, "An analytical model for short-channel organic thin-film transistors," *J. Appl. Phys.*, vol. 78, no. 2, p. 1088, Jul. 1995.

[6] M. Estrada, I. Mejía, A. Cerdeira, J. Pallares, L. F. Marsal, and B. Iñiguez, "Mobility model for compact device modeling of OTFTs made with different materials," *Solid-State Electron.*, vol. 52, no. 5, pp. 787–794, May 2008.

[7] M. Estrada *et al.*, "Modeling the behavior of charge carrier mobility with temperature in thin-film polymeric transistors," *Microelectron. Eng.*, vol. 87, no. 12, pp. 2565–2570, Dec. 2010.

[8] A. Castro-Carranza *et al.*, "Effect of density of states on mobility in small-molecule n-type organic thin-film transistors based on a perylene diimide," *IEEE Electron Device Lett.*, vol. 33, no. 8, pp. 1201–1203, Aug. 2012.

[9] F. Torricelli, K. O'Neill, G. H. Gelinck, K. Myny, J. Genoe, and E. Cantatore, "Charge transport in organic transistors accounting for a wide distribution of carrier energies—Part II: TFT modeling," *IEEE Trans. Electron Devices*, vol. 59, no. 5, pp. 1520–1528, May 2012.

[10] J. D. Yuen *et al.*, "Nonlinear transport in semiconducting polymers at high carrier densities," *Nature Mater.*, vol. 8, pp. 572–575, Jun. 2009.

[11] K. Asadi, A. J. Kronemeijer, T. Cramer, L. J. A. Koster, P. W. M. Blom, and D. M. de Leeuw, "Polaron hopping mediated by nuclear tunnelling in semiconducting polymers at high carrier density," *Nature Commun.*, vol. 4, Apr. 2013, Art. no. 1710.

[12] O. Marinov, M. J. Deen, U. Zschieschang, and H. Klauk, "Organic thin-film transistors: Part I—Compact DC modeling," *IEEE Trans. Electron. Devices*, vol. 56, no. 12, pp. 2952–2961, Dec. 2009.

[13] C. H. Kim *et al.*, "A compact model for organic field-effect transistors with improved output asymptotic behaviors," *IEEE Trans. Electron Devices*, vol. 60, no. 3, pp. 1136–1141, Mar. 2013.

[14] A. Castro-Carranza *et al.*, "Compact capacitance model for OTFTs at low and medium frequencies," *IEEE Trans. Electron Devices*, vol. 61, no. 2, pp. 638–642, Feb. 2014.

[15] J. Zaumseil, K. W. Baldwin, and J. A. Rogers, "Contact resistance in organic transistors that use source and drain electrodes formed by soft contact lamination," *J. Appl. Phys.*, vol. 93, no. 10, pp. 6117–6124, May 2003.

[16] A. Valletta *et al.*, "Contact effects in high performance fully printed p-channel organic thin film transistors," *Appl. Phys. Lett.*, vol. 99, Dec. 2011, Art. no. 233309.

[17] P. Necliudov, M. Shur, D. Gundlach, and T. Jackson, "Modeling of organic thin film transistors of different designs," *J. Appl. Phys.*, vol. 88, no. 11, pp. 6594–6597, Sep. 2000.

[18] D. Gundlach, L. Zhou, J. A. Nichols, T. N. Jackson, P. V. Necliudov, and M. S. Shur, "An experimental study of contact effects in organic thin film transistors," *J. Appl. Phys.*, vol. 100, May 2006, Art. no. 024509.

[19] L. Bürgi, T. J. Richards, R. H. Friend, and H. Sirringhaus, "Close look at charge carrier injection in polymer field-effect transistors," *J. Appl. Phys.*, vol. 94, no. 9, pp. 6129–6137, Nov. 2003.

[20] J. Jang *et al.*, "Extraction of the sub-bandgap density-of-states in polymer thin-film transistors with the multi-frequency capacitance-voltage spectroscopy," *Appl. Phys. Lett.*, vol. 100, Mar. 2012, Art. no. 133506.

[21] J. Jang, J. Lee, H. Kim, S.-J. Choi, D. M. Kim, and D. H. Kim, "Density-of-states based numerical and analytical models for solution-processed polymer TFTs," in *Proc. 28th Int. Tech. Conf. Circuits/Syst., Comput. Commun. (ITC-CSCC)*, Yeosu, South Korea, 2013, pp. 357–359.

[22] J. Jang *et al.*, "Inkjet printed polymer SRAM-cell design for flexible FPGA with physical parameter-based TFT model," in *IEDM Tech. Dig.*, Dec. 2013, pp. 11.6.1–11.6.4.

[23] J. Lee *et al.*, "Reliable and uniform thin-film transistor arrays based on inkjet-printed polymer semiconductors for full color reflective displays," *Adv. Mater.*, vol. 25, no. 41, pp. 5886–5892, 2013.

[24] T. Leroux, "Static and dynamic analysis of amorphous-silicon field-effect transistors," *Solid-State Electron.*, vol. 29, no. 1, pp. 47–58, Jan. 1986.

[25] M. C. J. M. Vissenberg and M. Matters, "Theory of the field-effect mobility in amorphous organic transistors," *Phys. Rev. B, Condens. Matter*, vol. 57, no. 20, pp. 12964–12967, May 1998.

[26] L. Pautmeier, R. Richert, and H. Bässler, "Hopping in a Gaussian distribution of energy states: Transition from dispersive to non-dispersive transport," *Philos. Mag. Lett.*, vol. 59, no. 6, pp. 325–331, Jun. 1989.

[27] S. Lee *et al.*, "Modeling and characterization of metal-semiconductor-metal-based source-drain contacts in amorphous InGaZnO thin film transistors," *Appl. Phys. Lett.*, vol. 96, no. 11, Mar. 2010, Art. no. 113506.

[28] M. Bae *et al.*, "Analytical models for drain current and gate capacitance in amorphous InGaZnO thin-film transistors with effective carrier density," *IEEE Electron Device Lett.*, vol. 32, no. 11, pp. 1546–1548, Nov. 2011.